Gas-Liquid-Solid Three-Phase Catalyzed S-Methylation of Thiophenol with Dimethyl Carbonate in a Fixed-Bed Reactor: Catalytic Performances of Activated Alumina Supported Alkali Metal Carbonate Catalysts

Yuchen Wu, Fenghua Zhang, Fei Li*, Heng Jiang, Rui Wang, Hong Gong
College of Chemistry, Chemical Engineering and Environmental Engineering, Liaoning Shihua University, NO.1, West Dandong Road, Fushun 113001, Liaoning, People's Republic of China.
lnpulf@126.com*

(Received on 12th September 2019, accepted in revised form 11th August 2020)

Summary: The catalytic performances of activated alumina and its supported alkali metal carbonate catalysts for the reaction of thiophenol with dimethyl carbonate to prepare thioanisole (PhSMe) were investigated on a fixed bed reactor under the condition of atmospheric pressure. The properties of activated alumina and its loading alkali metal carbonate catalysts were characterized via IR, BET and XRD. The effect of loading amount of alkali metal carbonate, calcination temperature, reaction temperature and liquid volume hourly space velocity (LVHSV) of reactants on the catalytic performances of the catalysts was also examined. The yield of PhSMe was 93.5% when activated alumina was used as catalyst alone at 120 ℃, however, the catalytic activities of the catalysts after loading 5-15 wt% K_2CO_3 were greatly improved, and the yield of PhSMe was 99-100%. Compared to activated alumina, the catalytic performances of catalysts after loading different alkali metal carbonate are greatly improved. The improvement of catalytic performance can be attributed to that carbonate may occupy the Lewis acid sites of the activated alumina surface, making it easier for the catalyst to activate thiophenol, thus giving benzenethiolate a stronger nucleophilic attack ability. The results of FTIR analysis show that the characteristic peaks of carbonate are blue shifted, also indicating that carbonate reacted with the surface of activated alumina. The Lewis basic site on the surface of the activated alumina is believed to play a crucial role.

Keywords: Thiophenol, Thioanisole, Activated alumina, Alkali metal carbonate, Gas-liquid-solid three phase catalysis.

Introduction

Aryl sulfides are widely used as a raw material for medicines, agrichemicals, photopolymerization initiators, etc., or as herbicides, insecticides and various solvents etc. Typically, thioanisole is usually synthesized by methylating thiophenol using a methylation reagent such as dimethyl sulfate [1], methyl halide [2], Trimethylsulfonium hydroxide (Me_3SOH) [3], Trimethylselenonium hydroxide (Me_3SeOH) [4], dimethyl carbonate (DMC) [5-8]. Among these methylation reagents, DMC is considered to be a non-toxic, cost-effective, and environmentally friendly raw material [9]. However, since the above-described various methylation methods are a liquid phase batch reaction, it requires complicated separation and purification steps for isolating methyl phenyl sulfide from the reaction solution. It is necessary to detoxify the waste liquid and waste water generated in the process.

From an industrial point of view, a continuous catalytic reaction process using a heterogeneous catalyst in a fixed bed is a preferred option because of the comparative advantages in process economy, safety, process control and heat recovery compared to batch reactions [10]. In the continuous flow process, the reaction materials are continuously charged while the reaction products are continuously discharged. The composition, temperature and other state parameters of the material at any position in the reactor does not change with time when the operation reaches a steady state. Under batch reaction conditions, the reaction environment is constantly changed during the reaction. More precisely, if the continuous flow reactor is considered to be the ideal plug flow, there is no back mixing in the axial direction. Another advantage of heterogeneously catalyzed reactions is that they permit continuous processes to be run easily, thus allowing toxic compounds to be handled with maximum safety. Thiophenol (PhSH) is a highly toxic chemical material, and the maximum exposure limit recommended by the NIOSH is 0.1 ppm. The oral LD50 of rats is 46.2 mg/kg [11]. Therefore, it must be prevented from leaking during use. The probability of leakage in the batch reaction process is high, and the continuous reaction process can reduce the risk of leakage. For this reason, many highly toxic molecules currently under research, should be based on continuous catalytic processes in the future, even when small capacities are needed.

Continuous flow processes of heterogeneous catalysis for the gas-phase S-methylation of PhSH are relatively rare. Tundo et al have employed GL-PTC (Gas-Liquid Phase-Transfer Catalysis) conditions to

*To whom all correspondence should be addressed.

prepare thioanisole. The α-alumina (corundum) spheres coated with 5 wt% potassium carbonate (K_2CO_3) and 5 wt% PEG 6000 w used as catalysts to catalyze the reaction of PhSH with dimethyl carbonate (DMC) in a continuous flow fixed bed reactor at normal pressure and 180 °C [12]. Under the same conditions, the catalytic system is also suitable for catalyzing the reaction of thiophenol with trimethyl orthoformate [13]. The conversion of PhSH is higher than 99.5%. Various catalysts such as activated alumina, NaX and NaY zeolite have been reported for the S-methylation of PhSH with methanol at 270 °C [14,15]. Silica gel supported $[(Nb_6Cl_{12})Cl_2(H_2O)_4]\cdot 6H_2O$ clusters were also used as catalyst for the S-alkylation of PhSH with various alkylation agent such as primary alcohols with shorter alkyl chains, aliphatic ethers, dialkyl carbonates, orthoesters and alkyl halides in gas-phase above 250 °C under a hydrogen stream [16].

In this paper, the reaction of PhSH with DMC has been investigated using activated alumina supported alkali metal carbonate as catalysts under mild reaction conditions (atmospheric pressure, 120 °C) in a fixed bed reactor. The reaction actually takes place under gas-liquid-solid three-phase conditions. Compared with the gas-solid phase catalytic reaction at high temperature, the gas-liquid-solid three-phase reaction at lower temperature reduces the risk of carbon deposition leading to block catalytic active sites on the catalyst surface, and also reduces the risk of thermal deactivation due to catalyst sintering or the risk of deactivation caused by sublimation of the active ingredient.

Experimental

Materials

Activated alumina balls (2~3 mm diameter) were supplied from Zibo Nuoda Chemical Company, P. R. China, and used as catalyst and catalyst carrier, respectively. PhSH was prepared in our laboratory by heterogeneous catalytic reaction between phenol and H_2S. The purity of PhSH is 99.9% (gas chromatography) after vacuum rectification. Analytical grade alkali metal carbonate (M_2CO_3) and DMC were purchased from Aaladin Industrial Corporation, P. R. China.

Catalysts preparation

The activated alumina balls were crashed, sieved to 10~20 mesh and dried at 120 ºC for 24 h before use. The supported M_2CO_3 catalysts were prepared by incipient wetness impregnation. Catalysts with different loading amount of M_2CO_3 were obtained after drying at 120 ºC for 24 h, the supported M_2CO_3 catalyst was designated as x-MC/A-120, where x is loading amount of M_2CO_3 by mass fraction, A and MC represent activated alumina and M_2CO_3, respectively. Every catalyst was also calcined in a muffle furnace at 500 °C in air for 3 h, and designated as x-MC/A-500.

Characterization

The KBr pellet technique was applied for determining IR spectra of the catalyst samples using FTIR spectroscopy (Specrum GX FTIR spectrometer, Perkin-Elmer, USA). The wave number range was from 400 to 4000 cm^{-1} with a resolution of 4 cm^{-1}.

The adsorption/desorption isotherms of the catalyst samples were measured at -196 °C via nitrogen adsorption instrument (ASAP-2010, Micromeritics, USA). In this process, 0.15 g sample was placed in a quartz tube and maintained at 300 °C under <1.3 Pa for 360 min to remove the moisture. The isothermal adsorption curve was used to calculate the specific surface area, total pore volume and pore size distribution. The specific surface area was calculated by the Brunauer-Emmett-Teller (BET) formula, total pore volume and pore size distribution were obtained from the desorption branches of the isotherms using Barrett-Joyner-Halenda (BJH) method.

X-ray diffraction (XRD) patterns of the activated alumina and catalyst samples with different M_2CO_3 were characterized using X-ray diffractometer (Rigaku D/max-RB,Japan) with Cu-Kα radiation source at 40 kV voltage, and 100 mA current at room temperature. The scan mode was performed with step size 0.02° from 5° to 70° with scanning 2θ range.

Catalytic reaction test

The catalytic performances of active alumina and catalyst samples were tested by a lab scale fixed bed reactor. The schematic diagram of the lab scale fixed-bed reactor was presented in Scheme 1. The quartz tube (9 mm i.d. × 530 mm long) was installed vertically, and the temperature is controlled by an open type electric heating furnace. The solid catalyst particles (8.0 mL packing height 125 mm) were packed into the middle of the quartz tube and the remaining space was filled with inert alumina ceramic balls and quartz wool plugs. The catalytic reaction tests were carried out under following conditions: atmospheric pressure, reaction temperature was 80 ~ 200 °C. The mixed solution of PhSH dissolved in DMC (PhSH/DMC molar ratio = 1.0), and the liquid volume hourly space velocity (LVHSV) of mixed solution was 0.75 ~ 3.0 h^{-1}. The products derived from fixed-bed reactor was condensed in condenser and then introduced into collector. As shown in scheme 1, the

gaseous by-products CO_2 was discharged to the atmosphere via vent valve connected on the collector which assure the reaction pressure was approximate to atmospheric pressure. The analysis of product was carried out by gas chromatography. The relative content of each component in products was determined by area normalization method. The conversion of PhSH was determined as the ratio of the amount of PhSH that has converted to the amount that was introduced into the reactor, the yield of PhSMe was calculated via the ratio of the amount of desired product PhSMe to the PhSH introduced into the reactor.

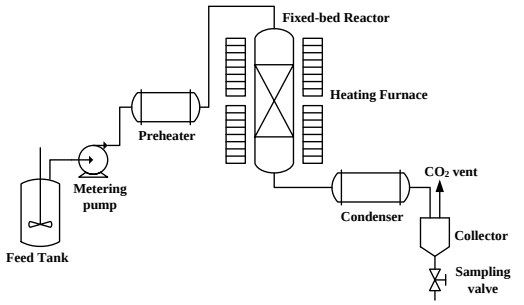

Scheme-1: Schematic diagram of the fixed-bed reactor system.

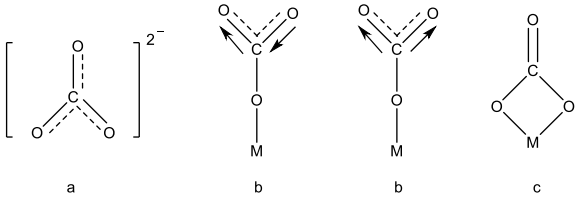

Scheme-2: The form of carbonate ions (M=metal). a: free carbonate ion, b: unidentate carbonate, c: bidentate carbonate.

Results and discussion

Catalyst characterization

Infrared spectroscopy analysis

Scheme 2 shows the three existing forms of CO_3^{2-}: free ions (symmetry D_{3h}), monodentate coordination (symmetry C_s), and bidentate coordination (symmetry C_{2v}) [17]. The infrared absorption band of CO_3^{2-} is closely related to its positional symmetry. The stretching vibration mode (ν3) is between 1530 and 1320 cm^{-1}. The ν3 bandwidth and absorption are the strongest, which is the characteristic absorption of carbonate. Pure K_2CO_3 is clearly monodentate coordination. The ν3 vibration mode of pure K_2CO_3 in Fig. 1 is split into two bands of 1457 cm^{-1} and 1382 cm^{-1}. When K_2CO_3 is loaded on the surface of the activated alumina carriers, the ν3 characteristic absorption peaks of CO_3^{2-} are blue-shifted (moving in the high wavenumber direction) to 1527 cm^{-1} and 1397 cm^{-1}, respectively, whether the catalysts were treated at 120 °C or 500 °C. The activated alumina carrier does not absorb at these two locations. This indicates that CO_3^{2-} has chemical interaction with the surface of the carrier, resulting in a change in the CO_3^{2-} coordination environment. The CO_3^{2-} after loading still belongs to the monodentate coordination. The peak at 1634 cm^{-1} of carrier itself is assigned to the bending vibration peak of the surface hydroxyl group. It can be seen from Fig. 1 that the peak intensity at 1634 cm^{-1} at 120 °C is was higher than that at 500 °C, which is attributed to the dehydration at high temperature resulting in the surface hydroxyl groups is reduced. Wang reported that γ-Al_2O_3 supported K_2CO_3 formed $KAl(OH)_2CO_3$ on the surface [18]. Although the surface texture properties of activated alumina and γ-Al_2O_3 are different, it is inferred from the FTIR results in Fig. 1 that K_2CO_3 has a chemical interaction with activated alumina. The FTIR spectra of supported Na_2CO_3, Rb_2CO_3 and Cs_2CO_3 (Fig. S1~Fig. S3) also show the same regularity as 5-15 KC/A. The CO_3^{2-} stretching vibration (ν3) comparison of pure M_2CO_3 and activated alumina supported M_2CO_3 is listed in Table-1.

Table-1: The CO_3^{2-} stretching vibration (ν3) comparison of pure M_2CO_3 and activated alumina supported M_2CO_3.

M_2CO_3	ν3 stretching vibration of CO_3^{2-} (cm^{-1})	
	Pure M_2CO_3	M_2CO_3/Al_2O_3 (1.45 mmol M/g)
Na_2CO_3	1435	1541, 1398
K_2CO_3	1457, 1382	1527, 1397
Rb_2CO_3	1448, 1372	1526, 1385
Cs_2CO_3	1450, 1373	1527, 1392

XRD analysis

The XRD patterns of the activated alumina carrier (0K/A) and catalysts with different K_2CO_3 loading amount are shown in Fig. 2. Under heat treatment conditions of 120 °C (Fig. 2A), both 0K/A and 5~15 wt% K_2CO_3 loading catalysts show two phases: boehmite (AlO(OH)) and γ-Al_2O_3. The crystallinity is low, and diffraction peaks of different intensities appear in the vicinity of 2θ = 14.4°, 28.2°, 37.7° and 49.3°, which are boehmite (AlO(OH)) characteristic peaks (JCPDS card number 83-2384). Diffraction peaks of different intensities appear in the vicinity of 2θ=37.4°, 45.8° and 67.2° belong to characteristic peaks of γ-Al_2O_3 (JCPDS card number 1-1303). Under heat treatment conditions of 500°C (Fig. 2B), whether 0K/A or 5~15 wt% K_2CO_3 loading samples, all of which show a single phase γ-Al_2O_3, indicating that the boehmite have decomposed at high temperature by dehydration. It can be seen from Fig. 2

that the characteristic diffraction peaks of K_2CO_3 are not found in the catalysts with K_2CO_3 loading amount of 5~15 wt%, indicating that K_2CO_3 is more uniformly dispersed in the pores of the activated alumina carrier and chemical interaction between K_2CO_3 and surface of carrier may occur. However, the species $KAl(OH)_2CO_3$ reported in the literature [18] is not observed in Fig. 2, which may be related to the nature of the carrier and the different preparation methods. The XRD patterns of catalysts supported Na_2CO_3, Rb_2CO_3 and Cs_2CO_3 (Fig. S4~Fig. S6) also show the same regularities as 5-15KC/A.

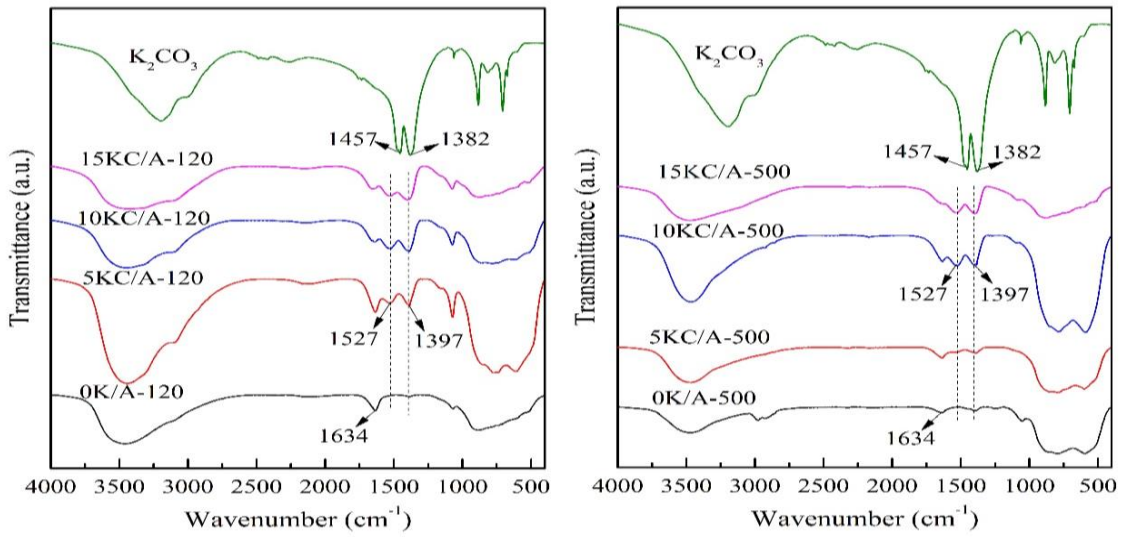

Fig. 1: FTIR spectra comparison of K_2CO_3 and catalyst samples with different K_2CO_3 loading amount after the heat treatment at 120 °C and 500 °C.

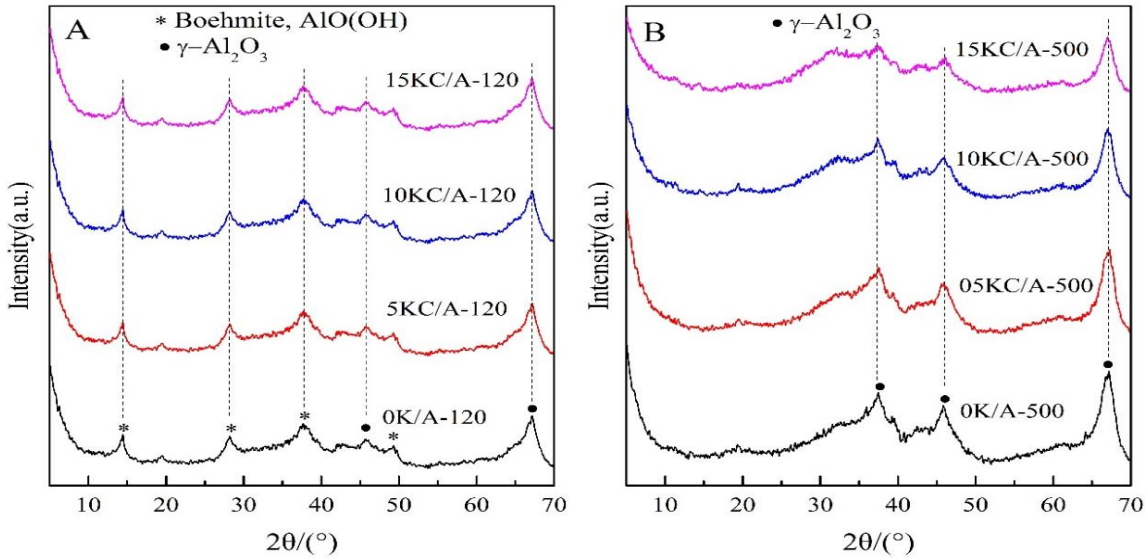

Fig. 2: The XRD patterns of activated alumina carrier (0K/A) and catalysts with different K_2CO_3 loading amount. A: dried at 120 °C; B: calcinated at 500 °C.

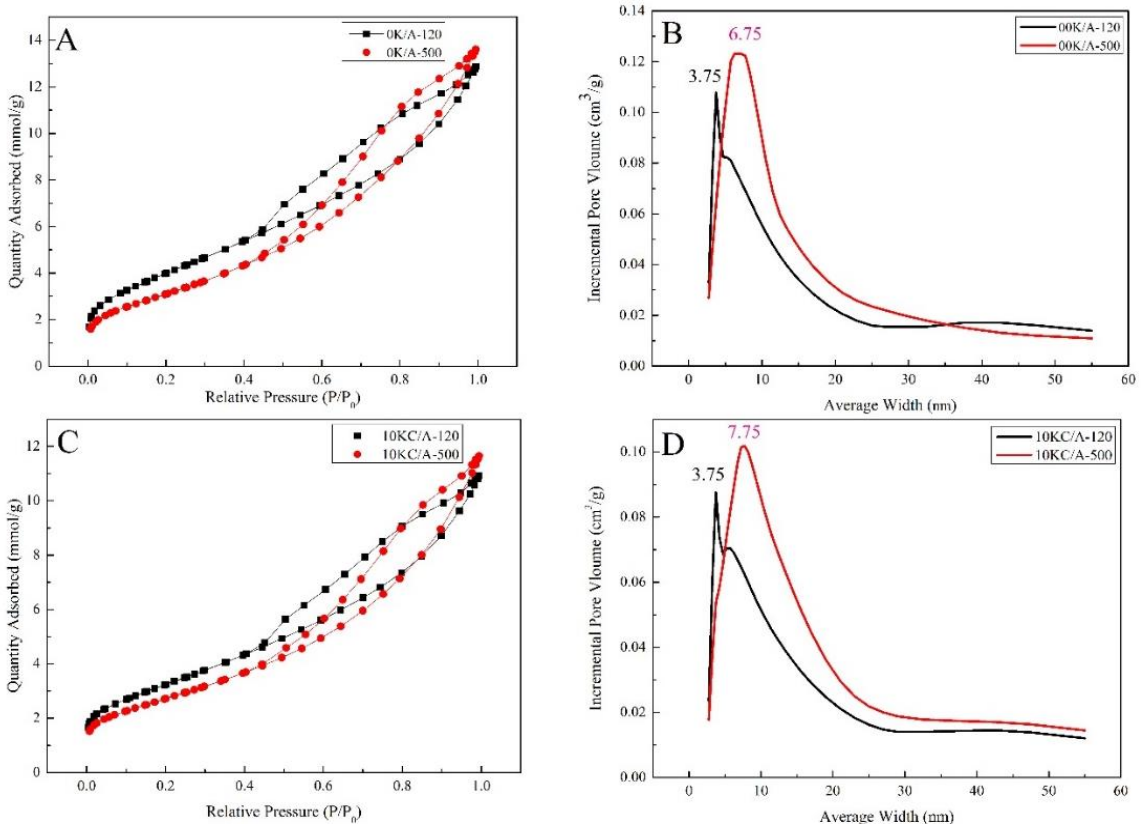

Fig. 3: N_2 adsorption–desorption isotherm (A and C) and BJH pore size distribution curves (B and D) for 0K/A and 10KC/A.

Table-2 Textural properties of 0K/A and 5~15 KC/A calcined at 120 °C and 500 °C

Catalysts	BET area (m^2/g)		Pore volume (mL/g)		Mean pore size diameter (nm)		Peak position in PSD (nm) [a]	
	120 °C	500 °C	120 °C	500 °C	120 °C	500 °C	120 °C	500 °C
0 K/A	**274**	**215**	**0.50**	**0.55**	**4.95**	**5.76**	**3.75**	**6.75**
5 KC/A	**255**	**214**	**0.46**	**0.51**	**4.98**	**5.66**	**3.75**	**5.75**
10 KC/A	**224**	**192**	**0.42**	**0.45**	**5.14**	**6.06**	**3.75**	**7.75**
15 KC/A	**165**	**130**	**0.36**	**0.36**	**5.33**	**6.40**	**3.75**	**8.75**

[a] PSD = pore size distributions

BET analysis

Fig. 3 shows a comparison of N_2 adsorption-desorption isotherms and BJH pore size distributions for 0K/A and 10KC/A. The adsorption-desorption isotherms of the two samples near $P/P_0 = 0$ are relatively flat, indicating that there are very few microporous structures in the sample. There is a significant hysteresis loop at $P/P_0 = 0.45$-0.99 (Fig. 3A and Fig. 3C). An increase in the amount of adsorption in the medium pressure region is interpreted as capillary condensation in the typical mesoporous materials. According to the IUPAC classification, the hysteresis loop belongs to the H3 type, and the corresponding pore type is slit-shaped pores [19]. The mesoporous size distribution of 0K/A at heat treatment conditions of 120 °C and 500 °C is 3.75-25 nm and 6.75-40 nm, respectively (Fig. 3B). The latter has a higher pore size distribution peak (7.75 nm) and is composed of richer mesopores. The reason for the increase in pore diameter after heat treatment at 500 °C is due to AlO(OH) dehydration and particle aggregation. The mesoporous size distributions of 10KC/A at heat treatment conditions of 120 °C and 500 °C are 3.75-29 nm and 7.75-32.5 nm, respectively (Fig. 3D). After 500 °C calcination, the pore size was further enlarged and had a relatively narrow distribution. After loading 10 wt% K_2CO_3, the smaller pores were filled with K_2CO_3. The adsorption-desorption isotherms and mesoporous size distribution of 5 KC/A and 15 KC/A under heat treatment conditions wether at 120 °C or 500 °C also showed the same regularity (Fig. S7).

Table-2 lists the relationship between the BET specific surface area, pore volume and average

pore size of the 0 K/A and 5~15 wt% K_2CO_3 loading catalysts, further confirming the conclusion of Fig. 3. 0 K/A-120 has a large specific surface area (274 m^2/g), and the specific surface area after calcination at 500 °C is reduced to 215 m^2/g. The pore volume, average pore diameter, and peak value of the pore size distribution of 0K/A-500 are increased as compared with 0 K/A-120. When the load is 5~15 wt% K_2CO_3, the specific surface area gradually decreases with the increase of the K_2CO_3 loading amount, indicating that K_2CO_3 occupies a part of the pores of the activated alumina carrier. The specific surface area after heat treatment at 500 ° C is smaller than that at the corresponding heat treatment of 120 °C. Compared with the heat treatment at 120 °C with 500 °C, the pore volume, average pore size and pore size distribution of 5~15 KC/A also show the same change with 0K/A.

Catalytic performance evaluation

Table-3 gives the effect of reaction temperature on the catalytic performances of 0 K/A-120 (activated alumina) and its supported K_2CO_3 catalysts. It can be seen from Table-3 that the PhSMe yield of 0K/A-120 at 80 °C is only 27.8%, while the PhSMe yields of 5KC/A-120, 10KC/A-120, and 15KC/A-120 are 48.8%, 75.7% and 76.6%, respectively. This indicates that the basic active sites of the catalyst surface play a crucial role, and the 10 wt% K_2CO_3 loading amount is enough to maintain the catalytic activity. With the increase of reaction temperature, the conversion rate of PhSH is also increasing. When the reaction temperature is 120 °C, the performances of the supported K_2CO_3 catalysts are closer to the theoretical value (PhSMe yield >99.6%), while the activity of 0K/A-120 catalyst is relatively low (PhSMe yield 93.5%). When the reaction temperature is in the range of 120~200 °C, the performances of the supported K_2CO_3 catalysts remain the maximum (PhSMe yield >99.8%), while the performance of the 0K/A-120 catalyst is also gradually increasing, but still weaker than the supported K_2CO_3 catalysts. Generally, solid base catalysts are sensitive to water and are easily poisoned by traces of water in air or raw materials. When the reaction temperature is lower than 100 °C, water molecules may occupy the active sites of the catalyst surfaces. Therefore, the reaction temperature is preferably 120 °C to evaporate trace amount of water.

The boiling points of the reactants PhSH and DMC are 169 °C and 90 °C, respectively, while the products PhSMe and CH_3OH are 188 °C and 64.7 °C, respectively. When the reaction temperature was 120 °C, the raw material DMC and the by-product CH_3OH were both vaporized, and the raw material PhSH and the product PhSMe were not vaporized. Therefore, the reaction at 120 °C occurs under gas-liquid-solid three-phase conditions. Compared with the gas-solid phase catalytic reaction at high temperature, the heat capacity of the liquid phase is large, and the reaction temperature can be kept constant, and that the reaction temperature is relatively low, which avoiding the risk of catalyst deactivation due to the occurrence of side reaction such as carbon deposition is also lowered, and lower reaction temperature is beneficial to maintain the activity, selectivity and stability of the catalyst under long-term continuous operating conditions.

Table-3: Effect of reaction temperatures on the catalytic performances of 0K/A-120 and supported K_2CO_3 catalysts dried at 120 °C. [a]

Reaction Temperature (°C)	PhSH Conversion（PhSMe Selectivity）			
	0 K/A-120	5 KC/A-120	10 KC/A-120	15 KC/A-120
80	27.8(100)	48.8(100)	75.7(100)	76.6(100)
100	79.2(100)	93.4(100)	92.5(100)	92.3(100)
120	93.5(100)	99.6(100)	99.8(100)	99.9(100)
140	97.3(100)	99.8(100)	99.9(100)	99.9(100)
160	97.9(99.8)	99.9(100)	99.8(100)	99.8(100)
180	98.1(99.9)	99.9(100)	99.9(100)	99.9(100)
200	98.6(99.8)	99.9(100)	99.9(99.9)	100(99.9)

[a] LVHSV = 0.75 h^{-1}, the reaction was carried out for 2 h at each temperature

Table-4 lists the comparative results of the catalytic performances of the 0 K/A and supported K_2CO_3 catalysts calcined at 500 °C. Comparing the results of Tables-3and 4, it can be seen for 0 K/A that the catalytic performance after heat treatment at 500 °C is lower than that of heat treatment at 120 °C. For 5~15 KC/A, the catalytic performances after heat treatment at 500 °C are slightly better than that at 120 °C, and the effect of K_2CO_3 loading amount on catalytic performance is not obvious.

.Table-4: Effect of reaction temperatures on the catalytic activities of 0K/A-500 and supported K_2CO_3 catalysts calcined at 500 °C [a]

Reaction Temperature (°C)	PhSH Conversion (PhSMe Selectivity) %			
	0 K/A-500	5 KC/A-500	10 KC/A-500	15 KC/A-500
120	91.4(100)	99.7(100)	100(100)	100(100)
140	91.0(99.9)	99.9(100)	100(100)	100(100)
160	84.0(99.9)	99.4(100)	99.8(100)	99.5(100)
180	83.8(100)	99.9(100)	100(100)	100(99.9)
200	93.9(100)	100(100)	100(99.9)	100(99.8)

[a] LVHSV = 0.75 h^{-1}, the reaction was carried out for 2 h at each temperature.

It is well known that the acidity of PhSH is relatively strong (p*K*a = 6.61) [20]. The basic sites on the catalyst surface can easily activate PhSH to produce PhS^- anion, which shows strong nucleophilic attack ability, while the two symmetric methyl groups in the DMC molecule belong to the electron deficient centers. Therefore,

the PhS^- anion easily attacks the methyl carbon in the DMC molecule. Table-5 lists the effect of LVHSV on the catalytic performances of various catalysts at a reaction temperature of 120 °C. In general, the catalytic performances of various catalysts are significantly reduced with the space velocity increased from 0.75 h^{-1} to 3.0 h^{-1}. When the space velocity is large, the residence time of the reactants in the catalyst bed are short, and the basic sites of the catalyst surface cannot activate PhSH to generate PhS^- anion in time, so the bimolecular nucleophilic substitution reaction of the methyl group in the DMC molecule cannot be performed in time. The effect of LVHSV on the catalytic performance in Table-5 indicates that the reaction process may follow the Eley-Rideal mechanism [21], that is, the alkali sites of the catalyst surface only activated PhSH without activating DMC. When the loading of alkali metal M (M = Na, K, Rb, Cs) was 1.45 mmol/g, the catalytic activities of the four catalysts were not significantly different.

Table-5: Effect of LVHSV on the catalytic performances of 0K/A and MC/A[a]

Catalysts	M loading amount (mmol M/g)	PhSH Conversion (PhSMe Selectivity) %		
		0.75 h^{-1}	1.5 h^{-1}	3.0 h^{-1}
0 K/A-120	0	94.3(100)	77.5(100)	41.3(100)
0 K/A-500	0	90.2(100)	66.5(100)	32.6(100)
5 KC/A-120	0.72	99.6(100)	91.0(100)	56.2(100)
5 KC/A-500	0.72	100(100)	93.5(100)	60.7(100)
10 KC/A-120	1.45	99.8(100)	93.0(100)	64.5(100)
10 KC/A-500	1.45	100(100)	96.1(100)	68.8(100)
15 KC/A-120	2.17	99.9(100)	92.5(100)	67.6(100)
15 KC/A-500	2.17	100(100)	97.2(100)	73.9(100)
8 NaC/A-120	1.45	99.6(100)	96.5(100)	71.8(100)
8 NaC/A-500	1.45	98.1(100)	91.2(100)	60.9(100)
17 RbC/A-120	1.45	99.9(100)	95.0(100)	69.0(100)
17 RbC/A-500	1.45	99.7(100)	94.2(100)	69.5(100)
24 CsC/A-120	1.45	99.8(100)	89.8(100)	57.7(100)
24 CsC/A-500	1.45	99.8(100)	91.3(100)	61.3(100)

[a] Reaction temperature 120 °C, the reaction was carried out for 4 h at each LVHSV.

The stability of 10KC/A-120 was investigated by continuous operation for 168 h at 120 °C and LVHSV = 0.75 h^{-1}. The experimental results are shown in Fig. S8 by sampling and analysis every 12 h. As expected, the catalyst is very stable. Before 144 h, the yield of PhSMe was averagely stable at 99.8 %, and the yields at 156 h and 168 h decreased slightly, but still reached 99.5 %.

Mechanism discussion

Important industrial processes using activated alumina itself as a catalyst include alcohol dehydration and sulfur recovery (Claus process) [22]. Catalytic alcohol dehydration on activated alumina is one of the oldest catalytic processes. Although some physical properties of alumina catalysts have been well characterized, a large number of studies have been also published on the catalytic dehydration reaction of alumina, but the surface structure and chemical properties responsible for catalytic performance remain unclear. It seems very reasonable that upon heating, the adjacent hydroxyl groups on the alumina surface dehydrate to form coordinating unsaturated Al^{3+} ions and O^{2-} ions, as shown in Scheme-3(a). The coordination-unsaturated Al^{3+} ion is a strong nucleophile acceptor, especially in the case of tetrahedral coordination. The catalytically active sites of activated alumina may be related to the presence of Lewis acid and base pairs on its surface. Almost all research reports related to the dehydration of alumina at high temperatures are considered to be the surface acidity of activated alumina. [23, 24]. Activated alumina have been used as a highly efficient catalyst for the formation of catalytic peptide bonds under mild conditions (<100 ° C) [25-29]. The high catalytic efficiency of activated alumina may be related to the presence of alumina surface active Lewis acid and base pairs. Lewis acid and basic sites activate $-COO^-$ and $-NH_3^+$, respectively.

We believe that the Lewis basic sites on the activated alumina surface play a key role to activate PhSH. When activated alumina is used alone as catalyst, its catalytic performance is relatively low because the basic sites activate PhSH to produce PhS^- anion, but the adjacent acid sites coordinate with the sulfur atom in PhS^- (Scheme 3(b)), resulting in a weakened nucleophilic capability of PhS^-. However, when alkali metal carbonate was loaded, its catalytic performances were greatly improved. A reasonable explanation is that CO_3^{2-} may occupy the coordination-unsaturated Al^{3+} (Scheme 3(c)), and the alkali metal ion M^+ may combine with O^{2-}, leading to the basicity on the activated alumina surface is stronger. In this case, the activated PhS^- has a stronger nucleophilic capability (Scheme 3(d)), so that the catalytic performances of the catalysts are greatly improved. From the infrared spectrum analysis (Fig. 1 and Table-1), it can be also seen that the characteristic peak of CO_3^{2-} has undergone a blue shift, which also confirms that the carbonate has a chemical interaction with the alumina surface.

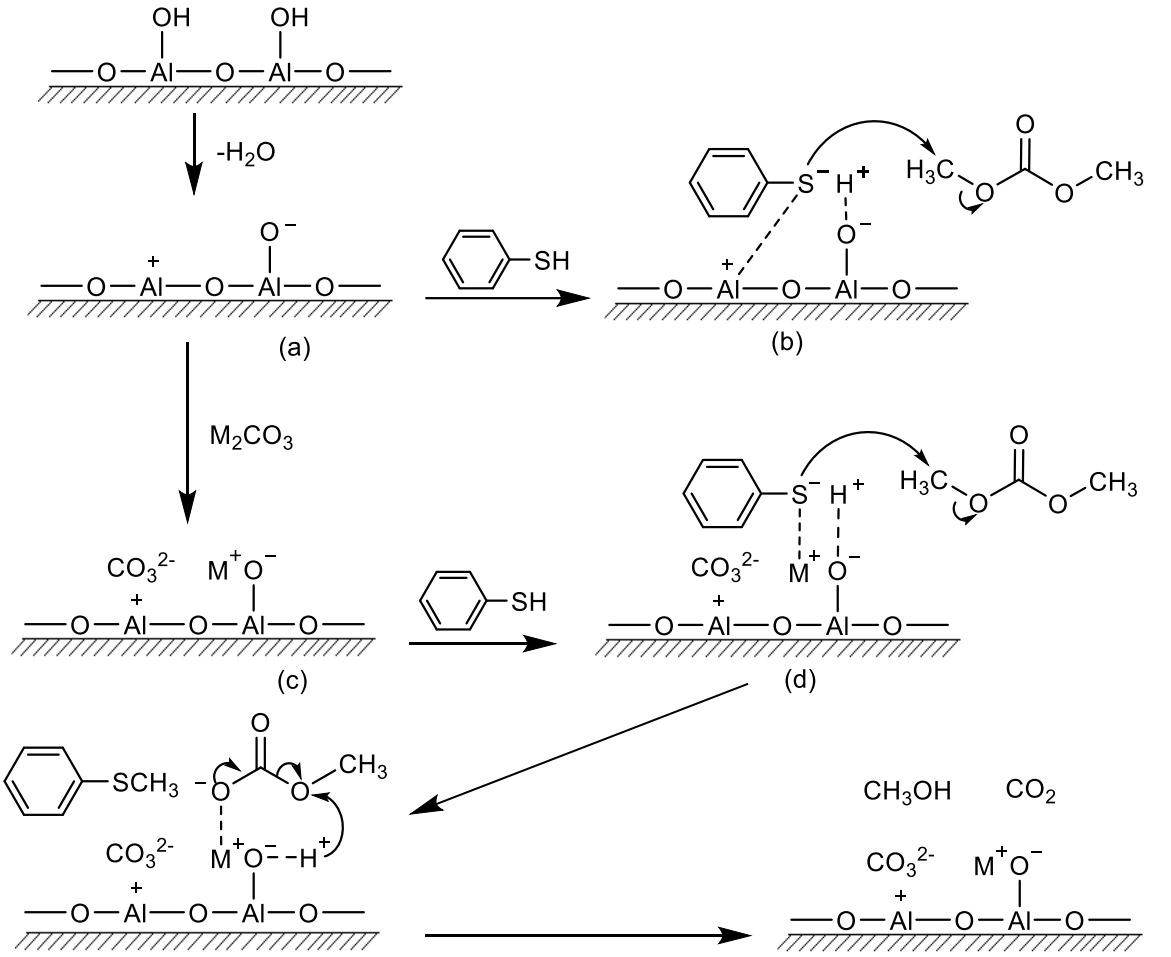

Scheme-3: Proposed catalytic reaction mechanism for activated alumina and its supported M_2CO_3 catalysts for S-methylation of PhSH with DMC. (a): The formation of Lewis acid and base sites on alumina surface; (b): The activation of PhSH on alumina surface; (c): CO_3^{2-} occupies the coordination unsaturated Al^{3+}; (d): Assumed mechanism of C−S bond formation on alumina supported K_2CO_3.

Conclusions

Thioanisole have been efficiently synthesized by S-methylation of PhSH with DMC using activated alumina supported alkali metal carbonate as catalysts in a fixed-bed reactor under gas-liquid-solid three-phase conditions at 120 °C. Under atmospheric pressure, the LVHSV of reactants solution (PHSH/DMC molar ratio = 1,) is 0.75 h^{-1}, the conversion of PhSH is more than 99 %, and the selectivity of thioanisole is 100 %.

The results of FTIR characterization indicate that there are some chemical interactions between CO_3^{2-} and activated alumina when the alkali metal carbonate is loaded onto the surface of activated alumina. The CO_3^{2-} ion may be coordinated with Al^{3+}, which occupies the acidic sites on the surface of the activated alumina. The basic sites of the catalyst surface play an important role for the catalytic reaction, and the catalytic performance of catalyst with alkali metal carbonate loading is greatly improved.

The reaction actually takes place under gas-liquid-solid three-phase conditions at 120 °C. Compared with the gas-solid phase catalytic reaction at high temperature, the lower reaction temperature also avoids the risk of deactivation of the catalyst due to carbon deposition at high temperature. Thus, it is ensured that the catalytic performance of the catalyst is not affected under long-term continuous operating conditions. The reaction process is continuous and the materials transport process is operated under sealed conditions, thereby avoiding the leakage risk of

PhSH during batch operation. Since the molar ratio of PhSH to DMC is stoichiometric, DMC and PhSH are almost completely converted, and by-products are methanol and CO_2, which do not require complicated separation and purification processes. Therefore, the reaction is non-polluting to the environment and a green, highly efficient thioanisole synthesis process.

Supplementary data

Electronic Supplementary Material associated with this article can be found in the online version of this paper.

Acknowledgment

This work was supported by Program for Liaoning Excellent Talents in University Educational Commission of Liaoning province of China (LR2018019).

References

1. M. M. Heravi, N. Z. Ahari, H. A. Oskooie, and M. Ghassemzadeh, Solid state S-methylation of thiols and O-methylation of phenols and naphthols with dimethyl sulfate under microwave irradiation, *Phosphorus Sulfur Silicon Relat Elem.*, **180**, 1701 (2005).
2. E. Voutyritsa, I. Triandafillidi, and C. G. Kokotos, Green organocatalytic oxidation of sulfides to sulfoxides and sulfones, *Synthesis.*, **49**, 917 (2017).
3. K. Yamauchi, T. Tanabe, and M. Kinoshita, Trimethylsulfonium hydroxide: a new methylating agent, *J Org Chem*., **44**, 638 (1979).
4. K. Yamauchi, K. Nakamura, and M. Kinoshita, Trimethylselenonium hydroxide: a new methylating agent. Tetrahedron Lett., **20**, 1787 (1979).
5. P. Tundo, L. Rossi, and A. Loris, Dimethyl carbonate as an ambident electrophile, *J Org Chem*., **70**, 2219 (2005).
6. T. Subramanian, A. Dhakshinamoorthy, and K. Pitchumani, Amino acid intercalated layered double hydroxide catalyzed chemoselective methylation of phenols and thiophenols with dimethyl carbonate, *Tetrahedron Lett*., **54**, 7167 (2013).
7. J. Xie, C. Wu, B. W. Christopher, J. Quan, and L. Zhu, Ionic Liquids-promoted S-methylation of thiols utilizing dimethyl carbonate. *Phosphorus Sulfur Silicon Relat Elem*., **186**, 31 (2011).
8. A. Dhakshinamoorthy, A. Sharmila, and K. Pitchumani, Layered double hydroxide-supported l-methionine-catalyzed chemoselective O-methylation of phenols and esterification of carboxylic acids with dimethyl carbonate: a "green" protocol, *Chem Eur J*., **16**, 1128 (2010).
9. G. Fiorani, A. Perosa, and M. Selva, Dimethyl carbonate: a versatile reagent for a sustainable valorization of renewables, *Green Chem.*,**20**, 288 (2018).
10. T. Glasnov, Continuous-Flow chemistry in the research laboratory, Amsterdam (Netherlands): Springer, p.1-5 (2016).
11. H. G. Shertzer. Organic sulfur compounds, in: Bingham E, Cohrssen B, Powell C editors. Patty's Toxicology, New York (NY): Wiley, p.1055-1056 (2012).
12. P. Tundo, F. Trotta, G. Moraglio, and F. Ligorati, Continuous-flow processes under gas-liquid phase-transfer catalysis (GL-PTC) conditions: the reaction of dialkyl carbonates with phenols, alcohols, and mercaptans, *Ind Eng Chem Res*., **27**, 1565 (1988).
13. M. Selva, F. Trotta, and P. Tundo, Esters and orthoesters as alkylating agents at high temperature. Applications to continuous-flow processes, *J Chem Soc Perkin Trans 2*., 519 (1992).
14. K. I. Areshidze, and M. K. Gadzhiev, Catalytic alkylation of thiophenol by methyl alcohol, *Soobshch Akad Nauk Gruz SSR*., **87**, 609 (1977).
15. O. Akira, and T. Shinichi, Method for producing alkylphenyl sulfide, Patent-JP2002371056A (2002).
16. S. Nagashima, K. Kudo, H. Yamazaki, S. Kamiguchib, and T. Chihara, Gas-phase S-alkylation of benzenethiol with aliphatic alcohols, ethers, esters, alkyl halides and olefins over halide cluster catalysts of Groups 5 and 6 transition metals, *Appl Catal A*., **450**, 50 (2013).
17. K. Nakamoto, Infrared and raman spectra of inorganic and coordination compounds, New York (NY): Wiley, p.1872-1892 (2002).
18. Y. Wang, J. Zhu, W. Huang, Synthesis and characterization of potassium-modified alumina superbases, *Phys Chem Chem Phys*., **3**, 2537 (2001).
19. K. S. W. Sing, Reporting physisorption data for gas/solid systems with special reference to the determination of surface area and porosity (Recommendations 1984), *Pure Appl Chem*., **57**, 603 (1985).
20. V. D. Bussolo, M. Caselli, M. R. Romano, M. Pineschi, and P. Crotti, Regio-and stereoselectivity of the addition of O-, S-, N-, and C-nucleophiles to the β vinyl oxirane derived from d-glucal. *J Org Chem*., **69**, 8702

(2004).
21. Y. Xiao, L. Gao, G. Xiao, and J. Lv, Kinetics of the transesterification reaction catalyzed by solid base in a fixed-bed reactor. *Energy Fuels.*, **24**, 5829 (2010).
22. L. K. Hudson, C. Misra, A. J. Perrotta, K. Wefers, and F. S. Williams, Aluminum oxide, Weinheim: Wiley, p.607-645 (2000).
23. A. Gervasini, G. Bellussi, J. Fenyvesi, and A. Auroux, Microcalorimetric and catalytic studies of the acidic character of modified metal oxide surfaces. 1. doping ions on alumina, magnesia, and silica, *J Phys Chem*., **99**, 5117 (1995).
24. C. Lahousse, F. Maugé, J. Bachelier, and J. Lavalley, Acidic and basic properties of titania-alumina mixed oxides; active sites for propan-2-ol dehydration, *J Chem Soc Faraday Trans*., **91**, 2907 (1995).
25. J. Bujdák, and B. M. Rode, Peptide bond formation on the surface of activated alumina: peptide chain elongation, *Catal Lett*., **91**, 149 (2003).
26. J. Bujdák, and B. M. Rode, Preferential amino acid sequences in alumina-catalyzed peptide bond formation. *J Inorg Biochem.*, **90**, 1 (2002).
27. S. Ghosh, A. Bhaumik, J. Mondal, A. Mallik, S. Sengupta (Bandyopadhyay), and C. Mukhopadhyay, Direct amide bond formation from carboxylic acids and amines using activated alumina balls as a new, convenient, clean, reusable and low cost heterogeneous catalyst, *Green Chem*., **14**, 3220 (2012).
28. J. Bujdák, and B. M. Rode, Silica, Alumina and clay catalyzed peptide bond formation: enhanced efficiency of alumina catalyst, *Origins Life Evol Biospheres*., **29**, 451 (1999).
29. A. Mondal, B. Banerjee, A. Bhaumik, and C. Mukhopadhyay, Activated alumina balls under neat conditions: a green catalyst for the synthesis of spiro-heterocyclic scaffolds by ring-opening versus annulation of the isatin moiety, *ChemCatChem*., **8**, 1185 (2016).